CHAPTER 4

RESULTS AND DISCUSSION

This chapter is composed of the calculation results and related discussion of the electronic structure, thermal properties; and thermoelectric properties of $CaMnO_3$ (CMO), C–substitute CMO, and CNTs–added CMO as follows:

Electronic structure

Electronic structure of $CaMnO_3$

Cluster atoms model

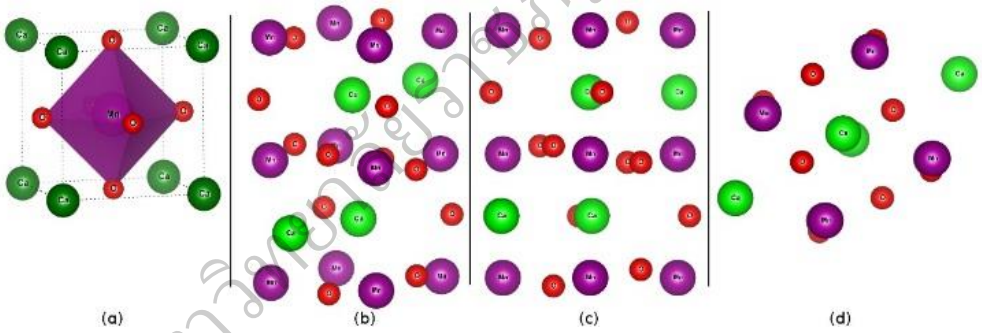

Figure 30 Cluster atoms model of $CaMnO_3$ showing (a) cubic structure and (b) orthorhombic structure, viewed in (c) 0 0 1 direction and (d) 0 1 0 direction

The cluster atoms model of CMO is color coded as Ca(green), Mn(purple), and O(red) in Figure 30. The CMO can be viewed through two structures; (1) the cubic structure (idealized cubic structure) (Reller et al., 1983, pp.913–914), and (2) orthorhombic structure (Sousa, et al., 2008, pp.311–319). These structures are exhibited differently and represent a unit cell. The cubic structure has 15 atoms viz., 8 Ca, 6 O atoms and a Mn atom, while the orthorhombic structure has 28 atoms

viz.,4 Ca atoms,12 O atoms and 12 Mn atoms. The unit cell volume of CMO is 51.89 $Å^3$ for the cubic structure and 207.75 $Å^3$ for the orthorhombic structure, (which is about 4 times larger than the cubic structure). The cluster model of CMO agrees well with the experimental data found in the literature (Reller et al., 1983, pp.913–914; Linh et al., 2010, pp.2–5; Zhang et al., 2011, pp.542–245; Zhang et al., 2011, pp.4171–4175; Zhang et al., 2011, pp.1258–1262; Seetawan, 2014, pp.9–14; Zhang et al., 2015, pp.1–5).

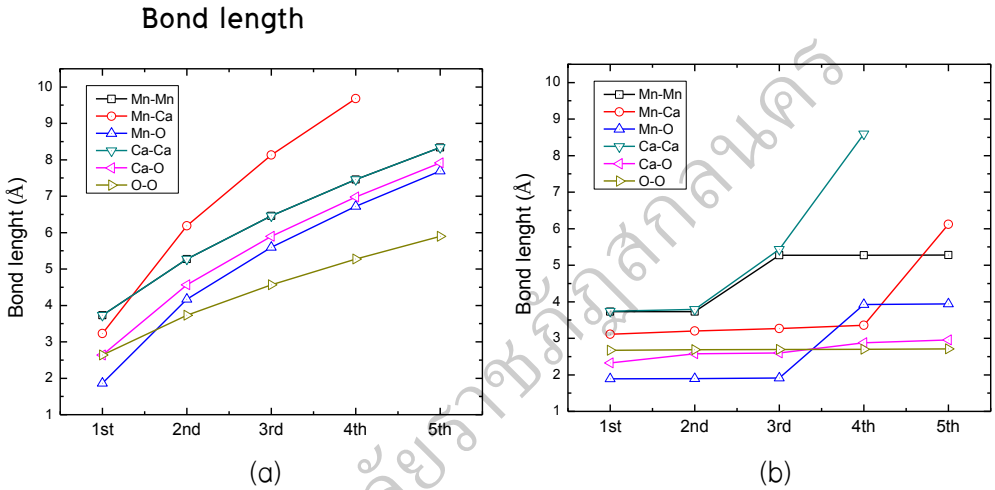

Figure 31 Bond length of CMO (a) cubic structure and (b) orthorhombic structure

The characteristic structure of CMO has been described by bond length distributions. The cubic structure showed an increasing distance for each order and this is consistent with the ideal cubic structure of CMO (Reller et al., 1983, pp. 913–914). The volume of the unit cell depended on the Mn–Mn and Ca–Ca bond length, as shown in Figure 31(a). The orthorhombic structure shows the atoms as closer neighbors than is the case with the cubic structure. The bonding of Ca–Ca, Mn–Ca and Mn–O are weak bonds at the 4^{th} order. However, the orthorhombic structure shows strong bonding as well as indicating good electrical conductance at the a– and c–axes (Zhang et al., 2015, pp. 1–5), as shown in Figure 31(b).

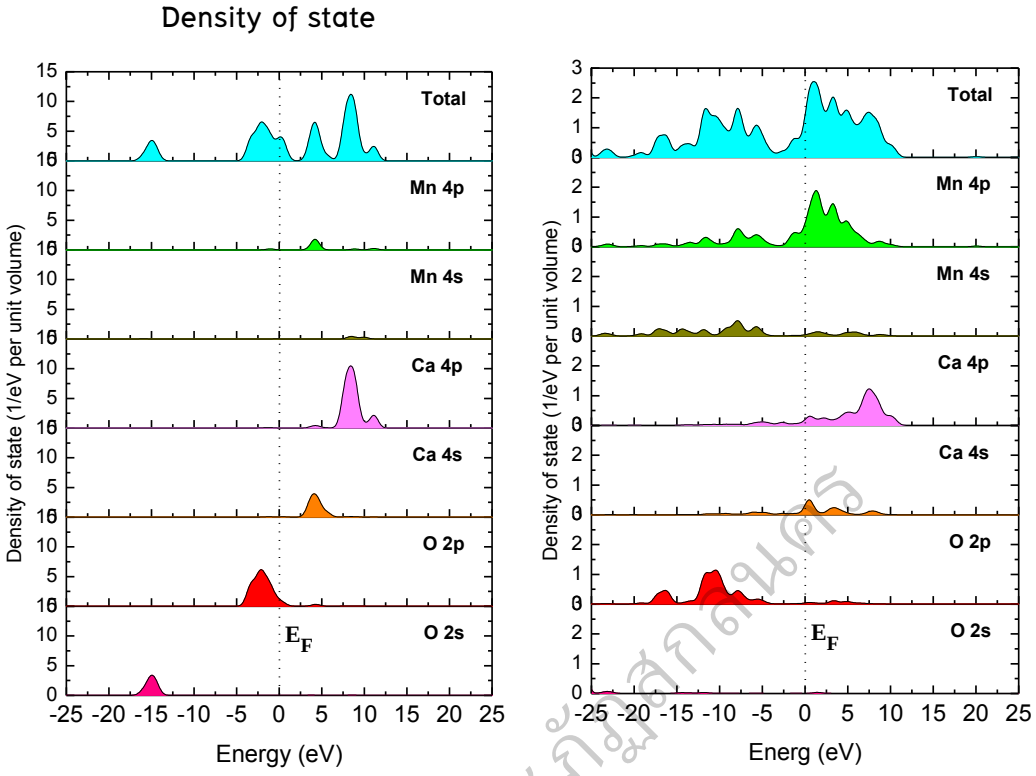

Figure 32 Density of state (DOS) of CMO (a) cubic structure and (b) orthorhombic structure

The DOS of CMO for both the cubic structure and orthorhombic structure are shown in Figure 32. These DOS values have demonstrated a difference of intensity depending on the number of atoms in the unit cell. The DOS intensity of the cubic structure has been shown to be larger than the orthorhombic structure, because the number of atoms in a unit cell with a cubic structure is less than a cell with on orthorhombic structure. The Seebeck coefficient and electrical conductivity in equation (3.2.3) and (3.2.4) with the complete number of orbitals (r), were obtained from the total peak in total DOS which was r =7 for the cubic structure and r =1.25 for the orthorhombic structure. The DOS of a CMO orthorhombic structure has O–orbitals which are in good agreement with the density functional theory (DFT) calculation, confirmed by Zhang et al. (2011, pp. 542–245). However, the Ca– and Mn–orbitals are not in agreement with DFT, because the DV–Xα method used the α

exchange correlation (α=0.7), based on the Hartree–Fock–approximation (Adach et al., 1978, pp. 875–883). On the other hand, the DFT calculation used the untra–soft pseudo–potential plan wave method and generalized gradient approximations (GGA) (Zhang et al., 2011, pp. 542–245). The DFT calculates in the Brillouin zone while DV–Xα calculates using sample points (cluster atom model). In addition, many interactions for pseudo–potential DFT were added in the self consistent field, while DV–Xα used Coulomb potential, Hartree potential and α exchange—correlation potential. Hence, the DFT calculation is an assumed all wave function and summation to calculate the electron density, but DV–Xα is calculated using all of the atoms, together with wave function to calculate the energy of the orbital for each atom. Therefore, it was found that different methods contributed to some different results.

Both DOS exhibited *n*–type thermoelectric materials, because of the number of total orbitals residing in the conduction band (positive value), which is accordance with recent work for DV–Xα (Rittiruam, Vora–ud, & Seetawan, 2015, pp. 1–4; Seetawan, Vora–Ud, Chainaronk, Thanachayanont, & Amornkitbamrung, 2010, pp. S225–S230; Vora–Ud, Seetawan, Jugsujinda, Thanachayanont, & Amornkitbamrung, 2012, pp. 868–879). In addition, the number of total orbitals for an orthorhombic structure near the Fermi level was shown to have high electrical conductivity, which later required confirmation by the energy gap.

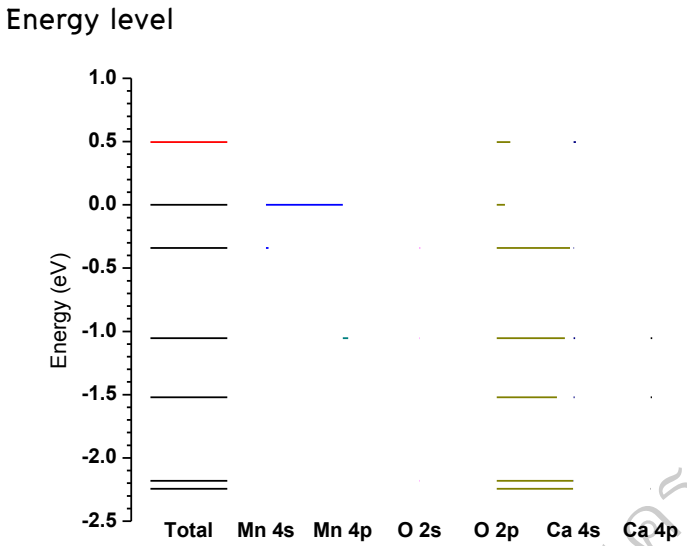

Figure 33 Energy level of CMO cubic structure

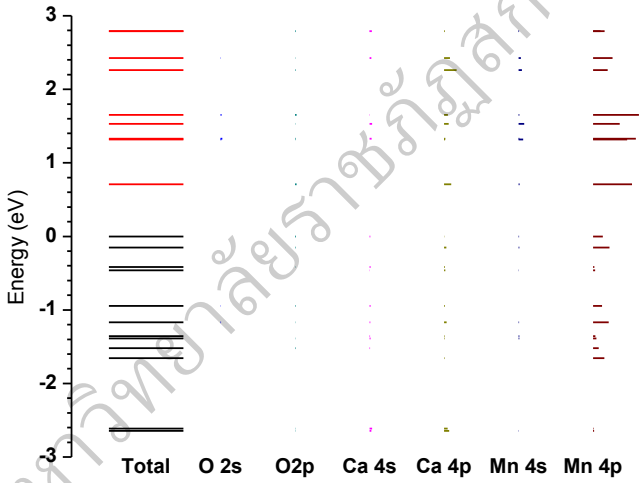

Figure 34 Energy level of CMO orthorhombic structure

The energy level of the cubic structure for CMO is shown in Figure 33. The energy level of the orthorhombic structure is shown in Figure 34. The accuracy of the calculated results can be confirmed by checking the energy gap in the energy level. The energy described in the conduction band is a positive energy value, while the valence band is a negative energy value. It can be seen that a cubic structure exhibits an energy gap of 0.5 eV, agreeing with the literature (0.4 eV) (Cardoso, Borges, Gasche, & Godinho, 2008, p. 035202). In an orthorhombic structure exhibited energy gap 0.7 eV which good agreement with several experiments and

calculations (Zhang et al. 2011, pp. 542–245; pp. 4171–4175; pp. 1258–1262; Seetawan, 2014, pp. 9–14; Zhang et al., 2015, pp. 1–5). Hence, the electronic structure of both the cubic and orthorhombic structures of CMO can be confirmed.

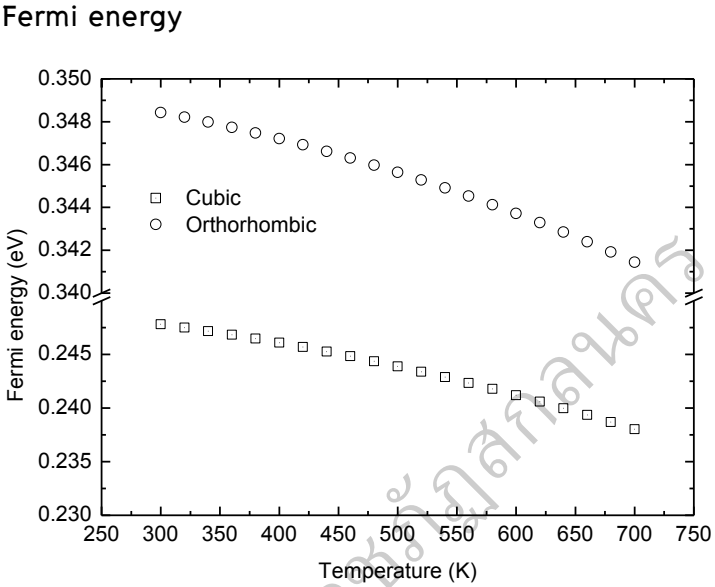

Figure 35 Fermi Energy of CMO cubic and orthorhombic structure various temperature

The Fermi energy of the cubic and orthorhombic structures of CMO is shown in Figure 35. The Fermi energy obtained was 0.24 eV for the cubic structure and 0.34 eV for the orthorhombic structure at room temperature. It can be observed that the Fermi energy slightly decreased with increasing temperature. It was predicted that the Seebeck coefficient and electrical conductivity will also decrease with increasing temperature

.

Electronics structure of CNTs-added $CaMnO_3$

Cluster atoms model

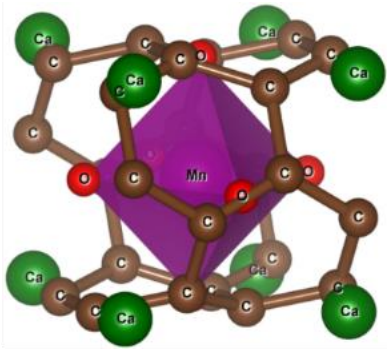

Figure 36 CNTs-added CMO cluster atoms model, color coded as Ca(green), Mn(purple), O(red), and C (brown)

The cluster atoms model of CMO in a unit cell and CNTs—added CMO with tubes 0.37 nm in diameter, 0.37 nm in length and 0.14 nm of atomic distance for Ca_8MnO_6, with 27(Oh) symmetries are shown in Figure 36. The CNTs significantly disturbed the structure of CMO, which affected the bond length in the cluster. However, this cluster was ignored during the phase change of the calculation process.

Bond length

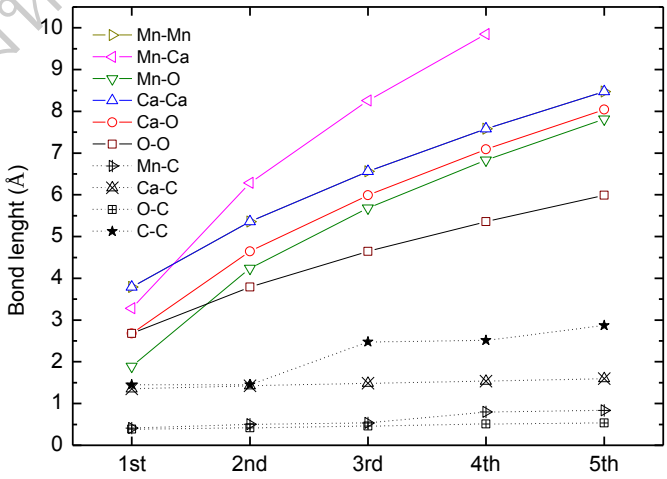

Figure 37 Bond length of CNTs-added CMO cluster atoms model

The close bond length distribution exhibited in C and residing in the unit cell are shown Figure 37. It should be confirmed again by experimentation. Such experimentation however is difficult. The character of CNTs–added materials can be confirmed by Tang et al. (2015, pp. 961–965). They successfully experimented with CNTs–added $Ca_3Co_4O_9$ which is based on Ca–Oxide material. In addition, the TEM image was evident when CNTs where added in $Ca_3Co_4O_9$.

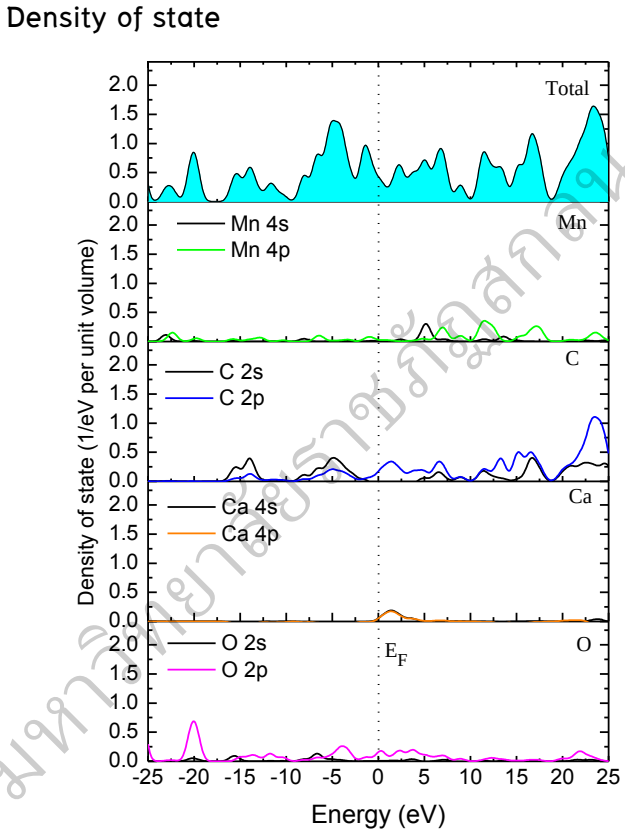

Figure 38 Density of state (DOS) of CNTs–added CMO cluster atoms model

The DOS of CNTs–added CMO is shown in Figure 38. The density of state reveals the energy intensity of the Mn– and Ca–orbitals as decreasing with the C–orbital increasing in energy intensity. It indicates that CNTs produce a carrier concentration which causes an increase in electrical conductivity and may decrease the Seebeck coefficient in some conditions (Tang et al., 2015, pp. 961–965; Lai et al.,

2015, p. 8120–4). In addition, the total DOS r =24.5 contributed to enhance the Seebeck coefficient and electrical conductivity.

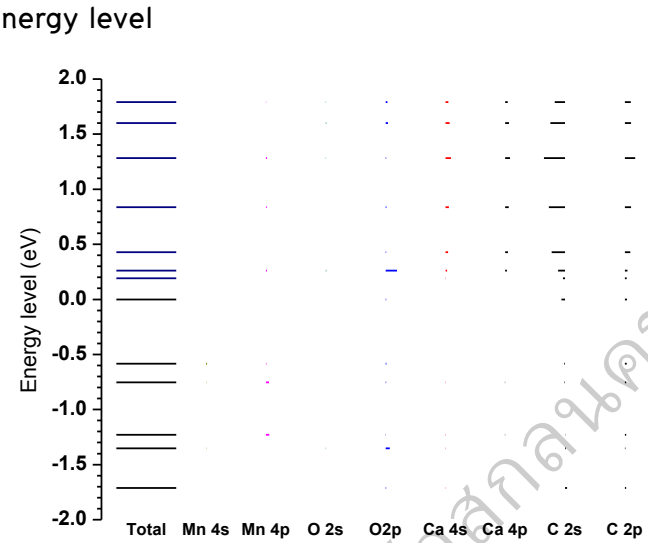

Figure 39 Energy level of CNTs–added CMO cluster atoms model

It can be seen that the energy gap of CNTs–added CMO is 0.19 eV, which is less than CMO (0.5 eV for a cubic and 0.7 eV for an orthorhombic structure). Because of the CNTs added to the unit cell and the carrier concentration that arises, (see Figure 39), the total DOS is close to the Fermi level confirmed by Zhang et al. (2015, pp. 1–5).

Fermi energy

The Fermi energy of CNTs–added CMO across a range of temperatures is shown in Figure 40. The Fermi energy value is 0.089 eV at room temperature compared with CMO. The Fermi energy has been decreased with the addition of CNTs, due to the energy gap being decreased. It should be expected that the Seebeck coefficient or electrical conductivity will be badly affected.

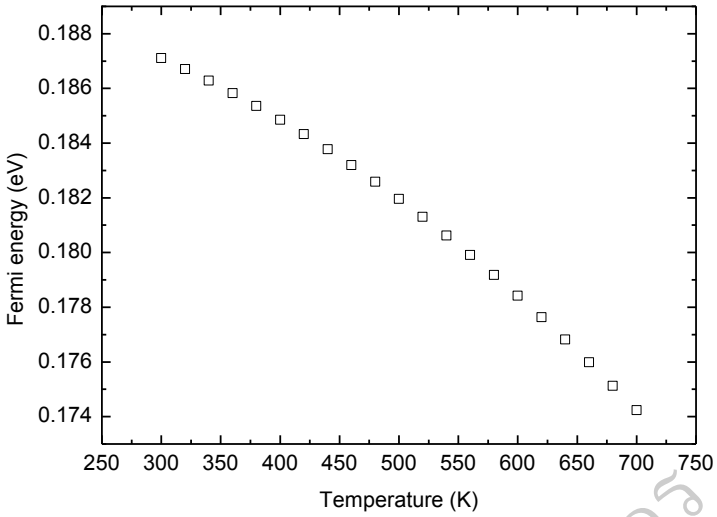

Figure 40 Fermi energy of CNTs-added CMO cluster atoms model various temperature

Electronics structure of C-substitute $CaMnO_3$

Cluster atoms model

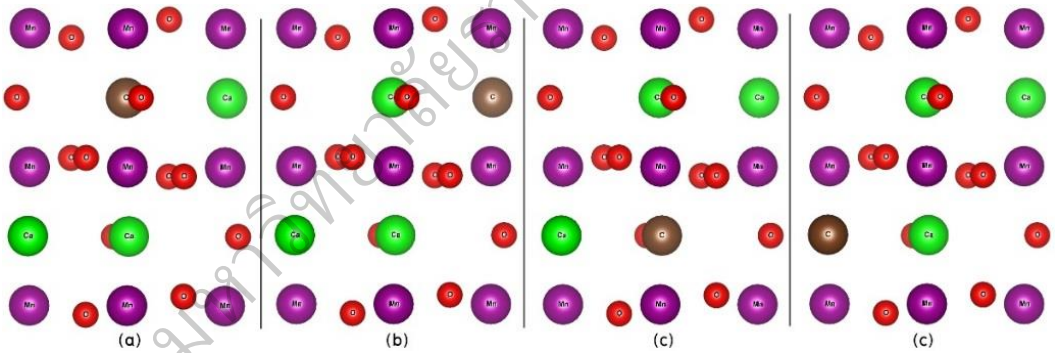

Figure 41 C-substitute CMO cluster atoms model (a) #1, (b) #2, (c) #3 and (d) #4 view 0 0 1 direction

The cluster atoms model of C-substitute CMO, illustrated with a color code given as Ca(green), Mn(purple), O(red), and C(wine) is shown in Figure 41. The possibility of a C-substitute in the A-site (Ca) was motivated by Lai et al. (2015, p. 8120-4). They used CNTs add in TiO_2 and found that C has a substitute Ti atom. The cluster atom models with a C-substitute CMO were separated into 4 cases, which in

cases #1 and #3 were similar and in cases #2 and #4 were similar. Note that, each cluster was calculated by ignoring the phase change.

Bond length

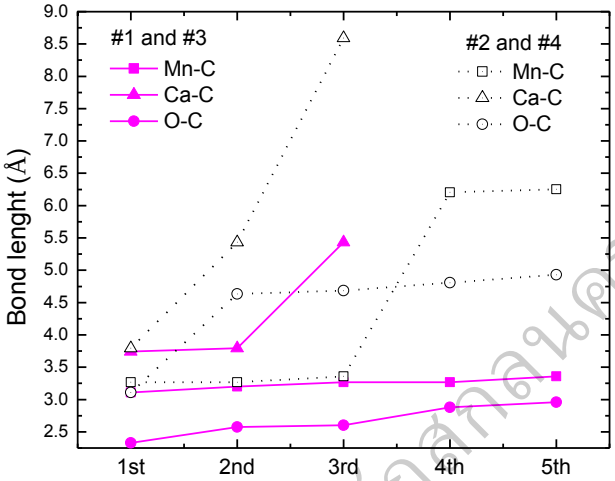

Figure 42 Bond length of C–substitute CMO cluster atoms model

The bond length of C–substitute CMO is shown in Figure 42. In cases #1 and #3, the bond length of Mn–, Ca–, and O–C exhibited strong bonding. This indicated that the unit cell has strong bonding. In cases #2 and #4, the bonding between Mn–, Ca–, and O–C was seen to be close in the first order, then at orders 2–5 it tended to be further apart.

Density of state

The DOS of C–substitute CMO is shown in Figure 43. The DOS exhibited in the C–orbital was of less intensity compared to the total DOS. The O–orbitals were observed to be still in the negative zone, while Ca–orbitals were still in the positive zone and a few changed intensity and shifted to nearly the Fermi level. It was found that the total DOS had increased energy intensity with a C–substitute, because C gives carrier concentration or carrier mobility to the Mn atoms, which causes an increase in the energy intensity of Mn–orbitals, as confirmed by Zhang et al. (2015, pp. 1–5). The number of total orbitals (r) can be obtained from the

combined peak in total DOS which was r ~0.5 for cases #1 and #3, then r ~0.3 for cases #2 and #4. It should be expected that a decreased Seebeck coefficient and possibly enhanced electrical conductivity will result. Furthermore, all cases exhibited the traits of *n*–type thermoelectric materials.

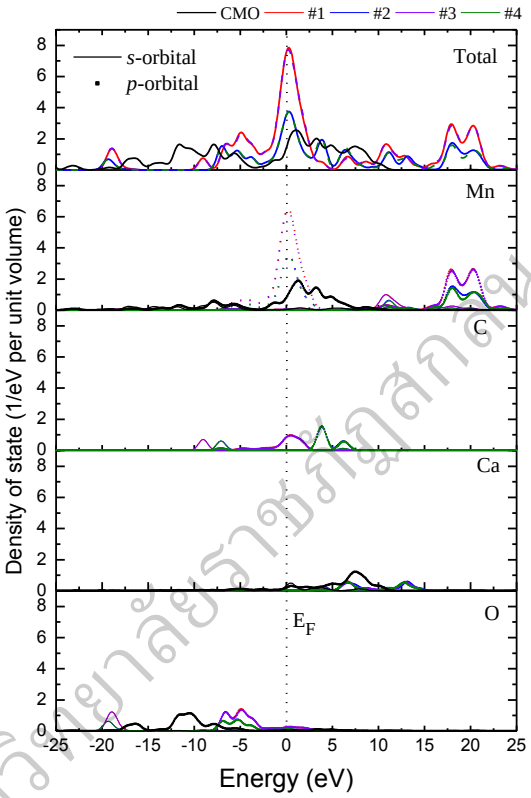

Figure 43 Density of state (DOS) of C–substitute $CaMnO_3$ cluster atoms model

Energy level

The energy level of C–substitute CMO is show in Figure 44. The energy level for four cases was compared with the energy level of a CMO orthorhombic. The valence band in the negative zone and the conduction band in the positive zone were obtained. It was found that C can reduce the energy gap from 0.7 eV to 0.03–0.04 eV. It may be that C atoms give an electron or carrier to Mn, which according to the DOS (See Figure 44), gives rise to an increase in the energy intensity

of the Mn–orbital. Moreover, in the case of C–substitute TiO_2 the C atoms decreased the energy gap from 2.89 – 1.67 eV (Lai et al., 2015, p. 8120–4).

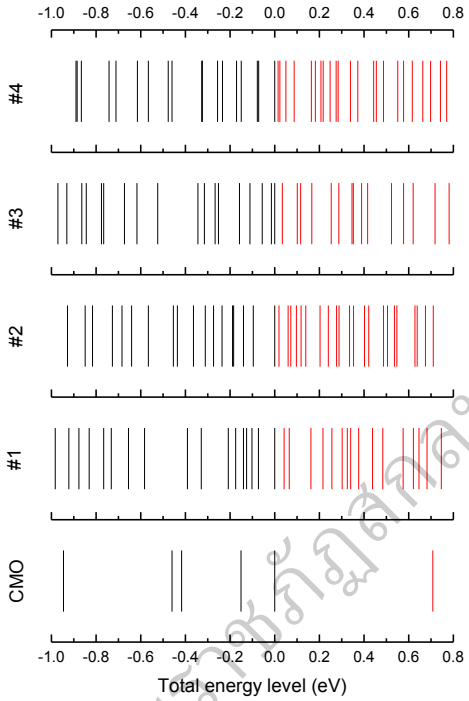

Figure 44 Energy level of C–substitute CMO cluster atoms model

Fermi energy

The Fermi energy of C–substitute CMO is shown in Figure 45. The Fermi energy reached a value of 0.24 eV for case #1, 0.23 eV for case #3, 0.14 eV for case #2 and 0.12 eV for case #4 at room temperature, respectively. The CMO in cases #2 and #4 has shown the Fermi energy to be significantly less than the CMO in cases #1 and #3.

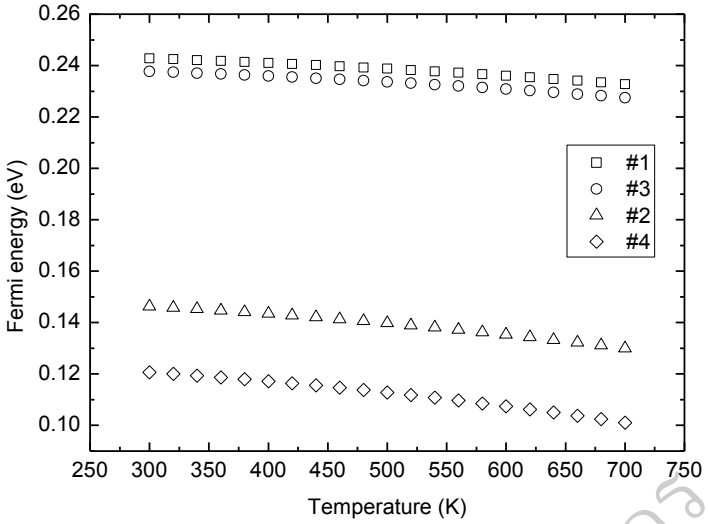

Figure 45 Fermi energy of C-substitute CMO cluster atoms model various temperature

Thermal properties

Cluster atoms model

The designed cluster atoms model of a CMO cubic structure with 320 atoms (Ca 64, Mn 64 and O 192 atoms), and a CMO orthorhombic structure with 240 atoms (Ca 52, Mn 60 and O 128 atoms) are shown in Figure. 46. The cluster atoms models were changed by a C-substitute in either the A-site or Ca-site. The choice of the sample case substitute was based on assumptions and knowledge around the probabilities and tendencies of thermal properties. Recently, the thermal properties of CMO in a cubic structure was carried out and reported (Rittiruam et al., 2014, pp. 585-593) and this was used to compare with the results. The designed CNTs-added CMO with a cluster totaling 247 atoms (Ca 64, Mn 27, O 108 and C 48 atoms) is shown in Figure. 47. This cluster was used to represent the CNTs-added structure of CMO. The cubic structure was chosen for these cases, because the thermal properties of cubic and orthorhombic structures are assimilative (Zhang et al., 2011, pp. 4171-4175; Seetawan, 2014, pp. 9-14; Rittiruam et al., 2014, pp. 585-593; Zhang et al., 2015, pp. 1-5).

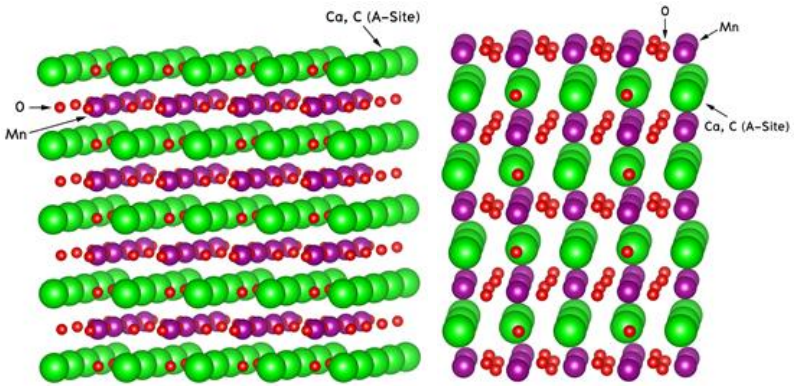

Figure 46 Cluster atoms model of CMO cubic structure (left) and CMO orthorhombic structure (right) for MD calculations

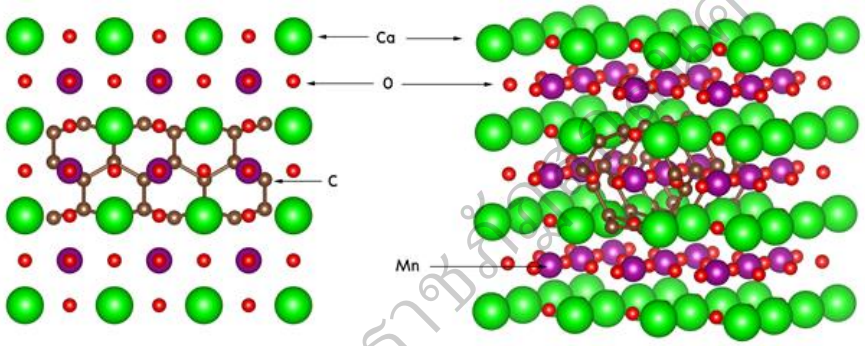

Figure 47 Cluster atoms model of CNTs-added CMO for MD calculations

Lattice parameter

The lattice parameter of C-substitute CMO and CNTs-added CMO were compared with previous work (Rittiruam, 2014, pp. 585-593) as shown in Figure 48. The lattice parameter of C-substitute CMO shows 0.3733 nm at 300 K. It was seen to slowly increase with increasing temperature. In addition, CNTs-added CMO shows a lattice parameter significantly more than CMO. It should be that the structure of CMO is harried. The lattice parameter has expanded with increasing temperature. These results should be checked for accuracy by experimentation again. However, the lattice parameter of two cases was investigated by standard MD and compared with experimentation. (Thongsri, et al., 2013, pp. 327-330; Rittiruam, 2014, pp. 585-593; Seetawan, 2014, pp. 9-14).

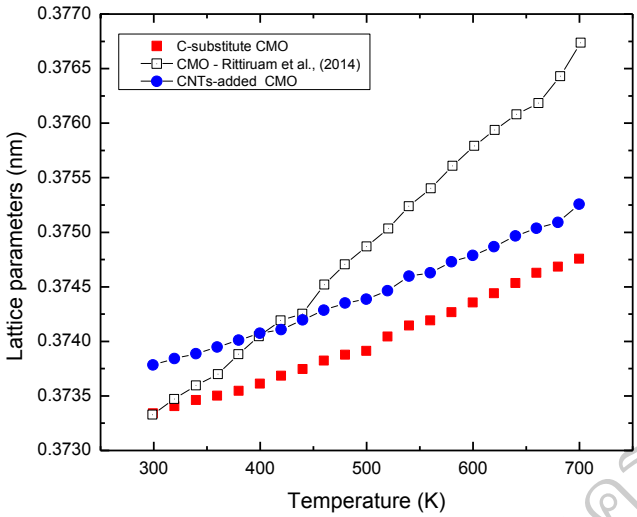

Figure 48 Lattice parameters of C–substitute CMO and CNTs–added CMO at various temperatures

Compressibility

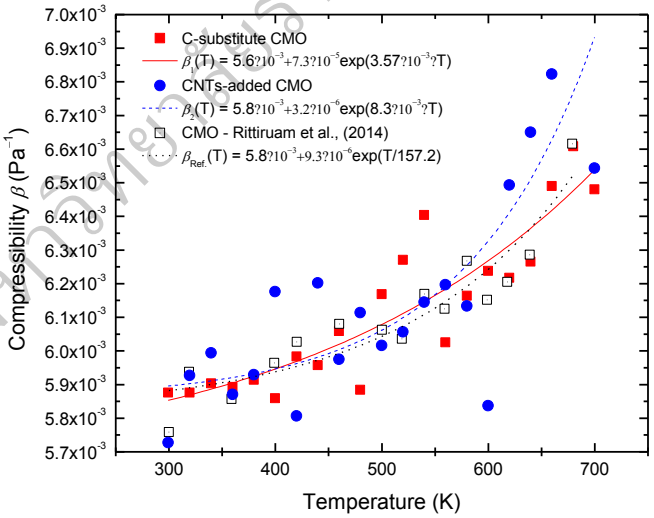

Figure 49 Compressibility of C–substitute CMO and CNTs–added CMO at various temperatures

The compressibility of C–substitute CMO and CNTs–added CMO is shown in Figure 49. The results were compared with previous work (Rittiruam, 2014, pp. 585–593) which agreed with changing compressibility at high temperature. It was

found that, the compressibility of CNTs–added CMO tended to increase better than CMO and C–substitute CMO.

Linear thermal expansion coefficient

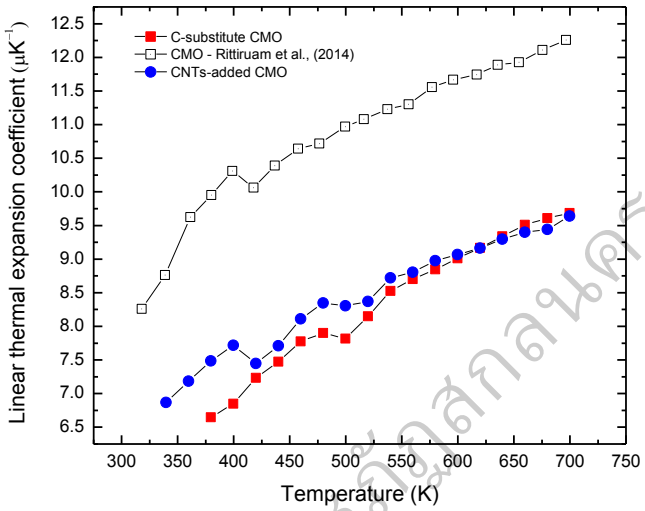

Figure 50 Linear thermal expansion coefficient of C–substitute CMO and CNTs–added CMO at various temperatures

The linear thermal expansion coefficients of C–substitute CMO and CNTs–added CMO are shown in Figure 50. Both of these coefficients have a value lower than that which was calculated for CMO. It was confirmed that the lattice expansion until structure expansion of C–substitute CMO and CNTs–added CMO slowly increases at high temperature.

Heat capacity

The heat capacity was composed of heat capacity at pressure constant (C_P), heat capacity at volume constant (C_V), and heat capacity of lattice dilatational term (C_d). The C_V obtained by the gradient of the internal energy is shown in Figure 51. The internal energy showed a difference at 300 K and tended towards the same value at 700 K. The compressibility and linear thermal expansion coefficient both

contributed to the evaluation of C_d. It was found that, our calculated heat capacity was lower than that calculated for CMO (Rittiruam, 2014, pp. 585–593). It is to be expected that the thermal conductivity of C–substitute CMO and CNTs–added CMO, is less than that of CMO. This is a result of C in the structure, (see Figure 51 and 52). In addition, the calculated result began to correspond with Dulong–Petit law at 450 K and clearly agreed with Dulong–Petit law at 600 K. It further indicated that at upper 600 K the thermal conductivity was a constant value.

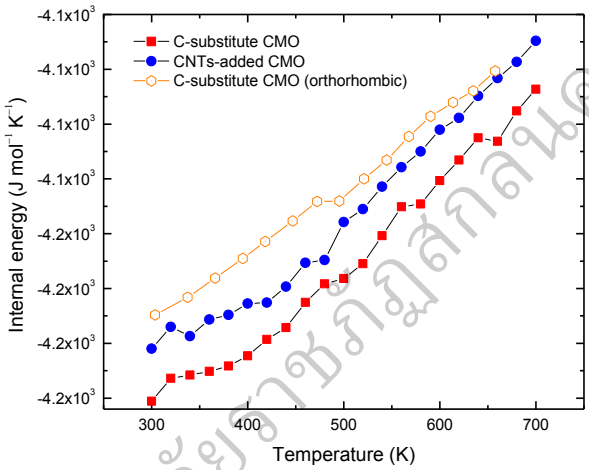

Figure 51 Internal energy of C–substitute CMO and CNTs–added CMO at various temperatures

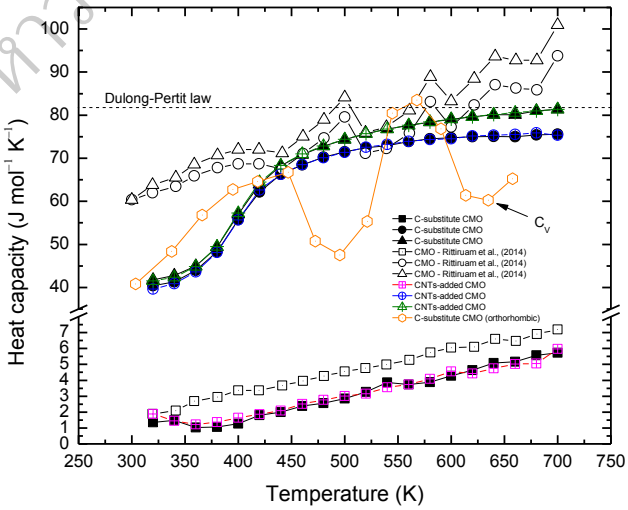

Figure 52 Heat capacity of C–substitute CMO and CNTs–added CMO various temperature

Auto-correlation function

The heat flux auto-correlation function and thermal conductivity of C-substitute CMO and CNTs-added CMO at various times are shown in Figure 53. It should be that the heat flux auto-correlation function has increased value with increasing temperature, while it's decay to zero with increasing temperature is also to be expected. It was indicated that at the point of first zero value can be found the relaxation time. The CNTs-added CMO has more heat flux auto-correlation function than did ours calculated at 700 K. The thermal conductivity showed decreased value, and quickly decayed to zero with increasing temperature. It correspondingly indicated lower thermal conductivity at high temperature.

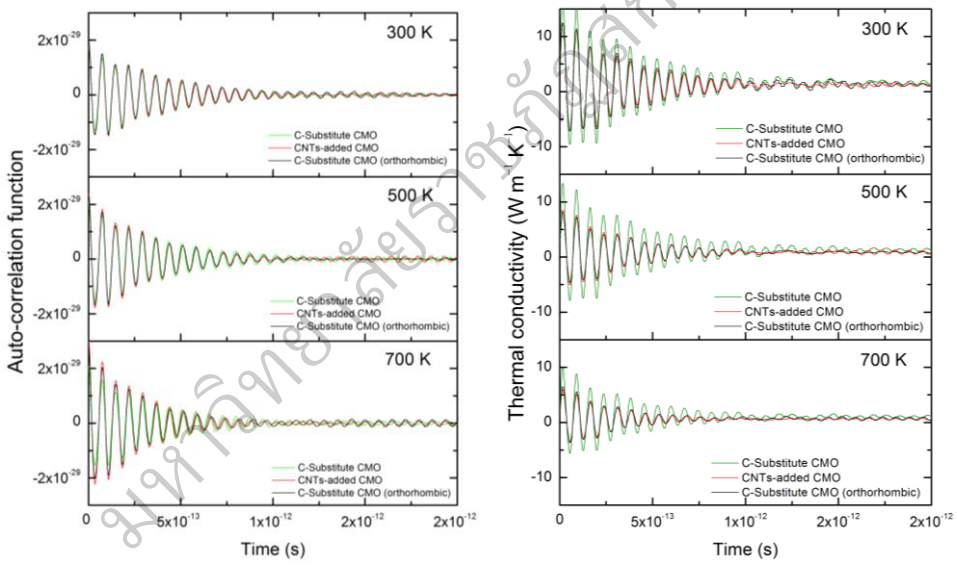

(a) (b)

Figure 53 Auto-correlation function and thermal conductivity of C-substitute CMO and CNTs-added CMO at various times

Thermoelectric properties

Thermoelectric properties of $CaMnO_3$

Seebeck coefficient

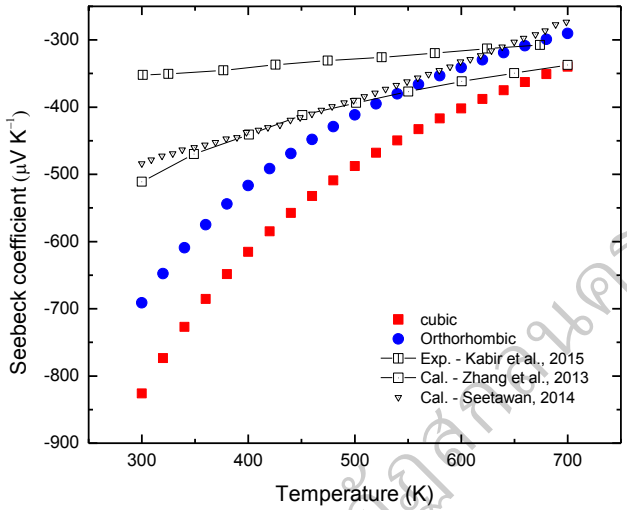

Figure 54 Seebeck coefficient of CMO at various temperatures

The Seebeck coefficients of the CMO cubic and orthorhombic structures are shown in Figure 54. The Seebeck coefficient shows a negative value in both cases and exhibits *n*–type semiconductor properties. (Ohtaki et al., 1995, pp. 105-111). The absolute Seebeck coefficient value is 825 $\mu V\ K^{-1}$ for the cubic structure and 691 $\mu V\ K^{-1}$ for the orthorhombic structure at 300 K, respectively. These values are approximately 2 times larger than that which is stated in the literature. The absolute Seebeck coefficient exhibited semiconductor behavior at room temperature and a decreased value, whilst increasing the temperature caused a display of metallic behavior. This agreed with the experimental and calculation data (Kabir et al., 2015, pp. 347–351; Zhang et al., 2013, pp. 1859-1864; Seetawan, 2014; pp. 9–14). In addition, the absolute Seebeck coefficient of the CMO cubic structure was significantly greater than the CMO orthorhombic structure.

Electrical conductivity

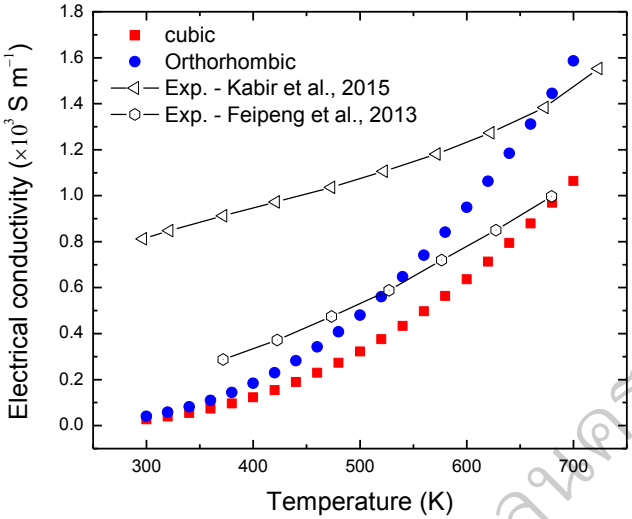

Figure 55 Electrical conductivity of CMO at various temperatures

The electrical conductivities of the CMO cubic and orthorhombic structures are shown in Figure 55. The calculated value is 27 S m^{-1} for the CMO cubic structure and 4 S m^{-1} for the CMO orthorhombic structure, each at 300 K. The calculated electrical conductivities agree with the experimental data (Kabir et al., 2015, pp. 347–351; Feipeng et al., 2013, pp. 885–890) i.e., semiconductor behavior as room temperature increased and with increasing temperature an indication of metallic behavior. The DOS and energy level have shown the total peak of DOS has near Fermi energy for the orthorhombic structure. Hence, the orthorhombic structure shows a lower Seebeck coefficient and more electrical conductivity than the cubic structure and it should possess better thermoelectric properties than the cubic structure, if thermal conductivity are the same.

Power factor

Before predicting the ZT value, the thermoelectric properties should be used to evaluate the power factor (PF) in order to check whether or not the materials exhibit good properties. (Ohtaki et al., 1995, pp. 105–111). The PF of both

cubic and orthorhombic structures show the same value at room temperature but slowly differentiate in value at upper 500 K temperatures. However, the calculated PF has a lower value than the experimental data (Kabir et al., 2015, pp. 347–351; Zhu et al., 2015, pp. 1535–1539). The PF shows good value in the order 10^{-6} which compares well with similarly conventional thermoelectric materials.

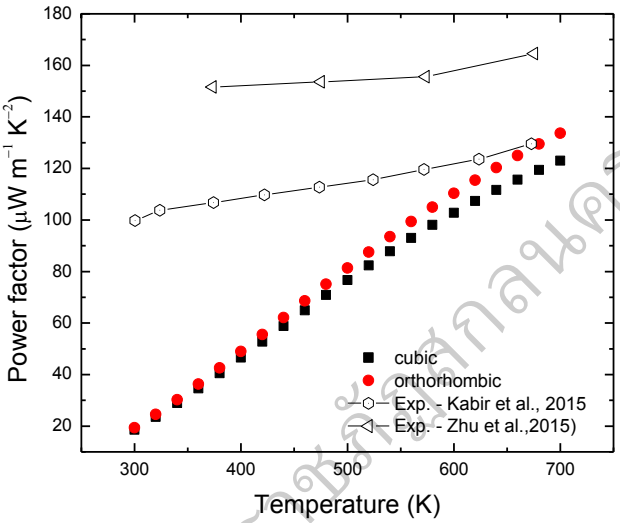

Figure 56 Power factor of CMO at various temperatures

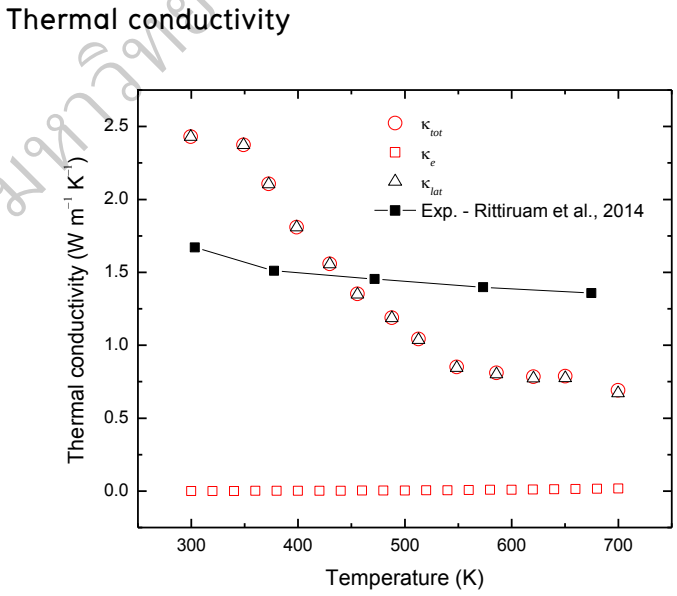

Figure 57 Thermal conductivity of CMO at various temperatures

The thermal conductivity relative to temperature was averaged out as shown by Figure 53. Figure 57 shows the electron thermal conductivity (κ_e), lattice thermal conductivity (κ_{lat}) and total thermal conductivity (κ_{tot}) of CMO. The κ_e has been a low value for both of the two structures, due to the electrical conductivity having the same value, while κ_{lat} is the same value, and the κ_{tot} is not different. In the recent instance, I successfully experimented and calculated the thermal conductivity, with the experiment showing κ_{tot} and the calculations showing κ_{lat}.(Rittiruam, et al., 2014, pp. 585–593). This confirmed that the thermal conductivity of the two structures is not different.

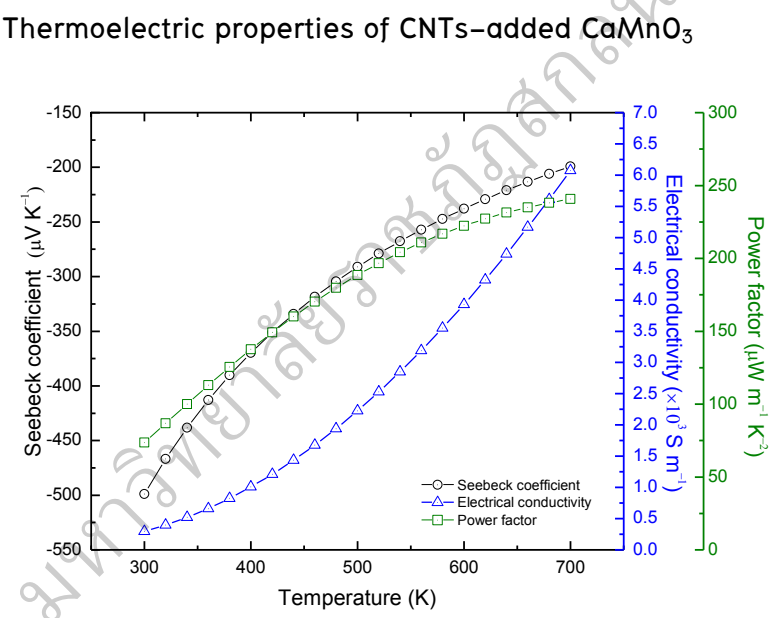

Figure 58 Seebeck coefficient, electrical conductivity and power factor of CNTs–added CMO at various temperatures

The thermoelectric properties comprised of Seebeck coefficient, electrical conductivity and power factor are shown in Figure 58. The Seebeck coefficient values show negative values which indicate an *n*–type thermoelectric material. The absolute Seebeck coefficient is 500 μV K^{-1}, the electrical conductivity is 2.9 $\times 10^2$ S m^{-1}, and the PF is 73×10^{-4} S m^{-1} at 300 K. Comparison of the thermoelectric properties of

CMO was examined and when the Seebeck coefficient decreased 50%, electrical conductivity was seen to increase 86% and PF increased 73% at 300 K.

The thermal conductivity of CNTs–added CMO together with the experimental data of Thongsri and Seetawan (2013, pp. 327–330) are shown in Figure 59. The κ_{tot} of CNTs–added CMO was 40% less than CMO. Because of the CNTs live in structure and hindrance which affects the heat flux auto–correlation, a quick decrease to zero was better with CMO. In addition, the κ_e of CNTs–added CMO was seen as small (Thongsri et al., 2013, pp. 327–330). The CNTs significantly improved the thermoelectric properties of CMO.

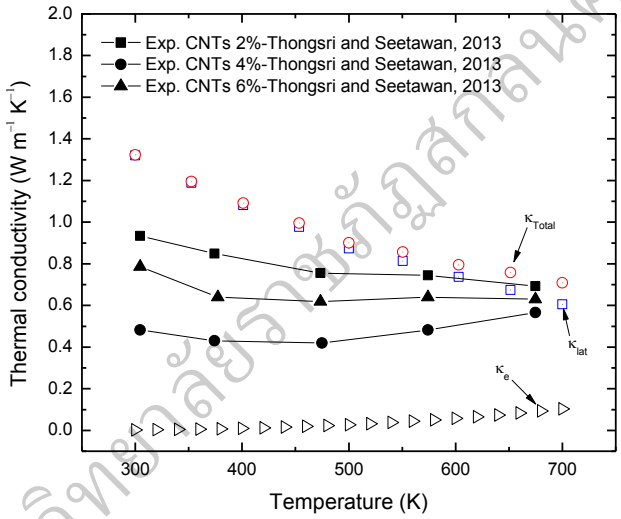

Figure 59 Thermal conductivity of CNTs–added CMO at various temperatures

Thermoelectric properties of C–substitute $CaMnO_3$

The **C–substitute $CaMnO_3$** was separated into four cases; #1, #2, #3, and #4, respectively. In terms of electronic structure, case #1 and #3 are similar, and #2 and #4 show similarities to each other. The thermoelectric properties can be described as follows;

Seebeck coefficient

The Seebeck coefficient of C–substitute CMO is shown in Figure 60. The absolute Seebeck coefficient is 674 $\mu V\ K^{-1}$ for case #1 and 660 $\mu V\ K^{-1}$ for case

#3 at 300 K, and the absolute Seebeck coefficient is 406 $\mu V\ K^{-1}$ for case #2 and 401 $\mu V\ K^{-1}$ for case #4 at 300 K, respectively. The calculated Seebeck coefficient of CMO saw the Seebeck coefficient reduced 2% for case #1, 41% for case #2, 4.4% for case #3 and 41% for case #4, respectively, with the addition of the C–substitute. However, the absolute Seebeck coefficient decreased with increasing temperature and displayed semiconductor behavior.

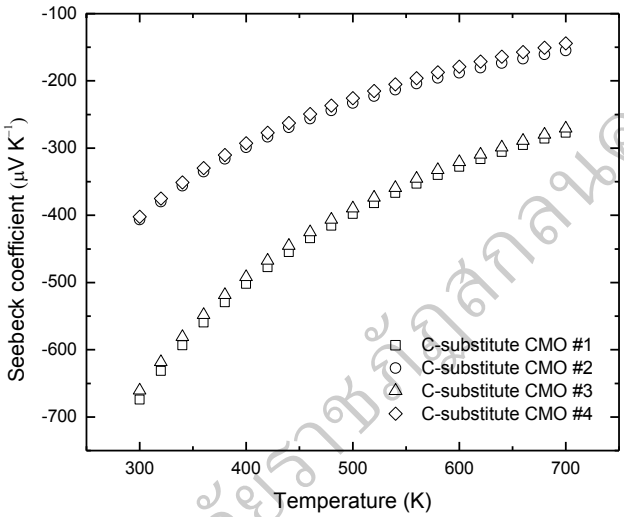

Figure 60 Seebeck coefficient of C–substitute CMO at various temperatures

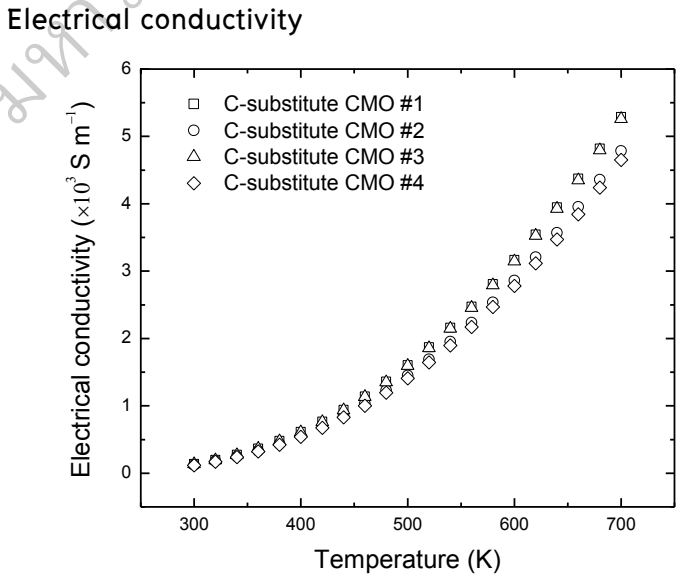

Figure 61 Electrical conductivity of C–substitute CMO at various temperatures

The electrical conductivity of C–substitute CMO is shown in Figure 61. The calculated results of CMO shows that C–substitute CMO has an enhanced electrical conductivity of 71% for cases #1 and #3; and 68% for cases #2 and #4, at 700 K, respectively. It is evident that the C significantly gives the concentration which agrees with the DOS (See Figure 43).

Power factor

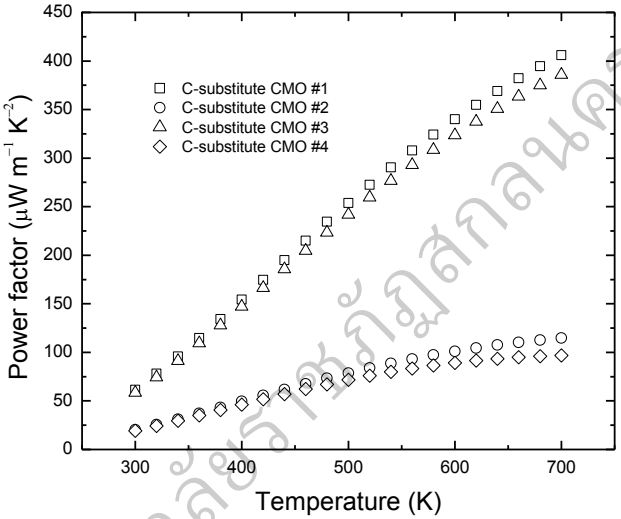

Figure 62 Power factor of C–substitute CMO at various temperatures

The power factor of the four separate cases of C–substitute CMO exhibited different values as shown in Figure 62. Cases #1 and #3 exhibited high power factors with values of 406 and 386 $\mu W\ m^{-1}\ K^{-2}$ respectively, both at 700 K. Cases #2 and #4 exhibited the lowest power factors which were similar to CMO. This also means that cases #1 and #3 should show high ZT values while cases #2 and #4 should show a ZT value the same as CMO.

Thermal conductivity

The thermal conductivity of C–substitute CMO is shown in Figure 63. The results of calculating the thermal conductivity of cases #1, #2, #3 and #4 show similar values to the CNTs–substitute at T = 300 – 450 K. They show a clear

difference in value however, at T = 450 – 700 K. The calculated result of CMO shows that the thermal conductivity has increased 9% for cases #1 and #3; and 8% for cases #2 and #4 at 700 K, respectively. Because the κ_e has increased, this indicates that the electrical conductivity has also increased.

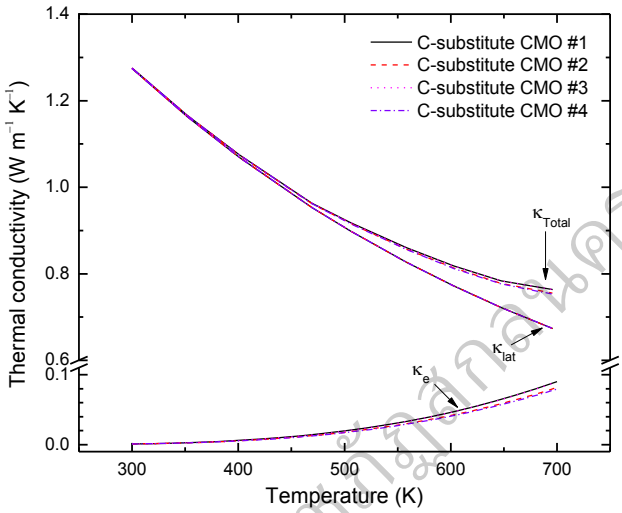

Figure 63 Thermal conductivity of C–substitute CMO at various temperatures

Dimensionless Figure of Merit

For the final result, the Dimensionless Figures of Merit (ZT) for all cases were compared with each other, as shown in Figure 64. To check the accuracycy of the calculations, the ZT of CMO with two structures was investigated and compared with data found in the relevant literature (Kabir et al., 2015, pp. 347–351; Zhu et al., 2015, pp. 105–109). The literature data showed ZT_{CMO} = 0.01 at 300 K, increasing to 0.03 – 0.04 at 700 K. The calculated results show the highest ZT_{CMO} = 0.12 at 700 K. Zhang et al. (2013, pp. 1859–1864) reported a calculation of ZT_{CMO}= 1.15 at 1000 K, which is higher than the experimental data also. In the cases concerning the CNTs–added CMO and C–substitute (case #1 and #3), a high ZT value of 0.18 – 0.2 at 700 K was observed. But in C–substitute cases #2 and #4, a ZT value of 0.06 at 700 K was observed and this did not improve the thermoelectric properties.

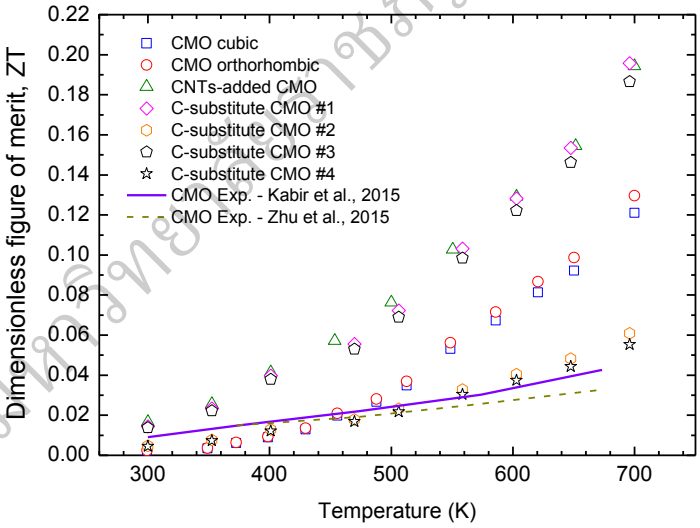

Figure 64 Dimensionless Figure of Merit (ZT) of CMO, CNTs–added CMO and C–substitute CMO at various temperatures